Supporting Information

A Sensitive and Reliable Organic Fluorescent Nanothermometer for Noninvasive Temperature Sensing

Ke Xue,[1] Chao Wang,[1] Jiaxin Wang,[1] Shuyi Lv,[1] Boyi Hao,[1] Chunlei Zhu,[1,*] and Ben Zhong Tang[2,3,*]

[1] Key Laboratory of Functional Polymer Materials of Ministry of Education, State Key Laboratory of Medicinal Chemical Biology, Institute of Polymer Chemistry, College of Chemistry, Nankai University, Tianjin 300071, China

[2] Shenzhen Institute of Aggregate Science and Technology, School of Science and Engineering, The Chinese University of Hong Kong, Shenzhen, Guangdong 518172, China

[3] Department of Chemistry, Hong Kong Branch of Chinese National Engineering Research Center for Tissue Restoration and Reconstruction, and Institute for Advanced Study, The Hong Kong University of Science and Technology, Clear Water Bay, Kowloon, Hong Kong, China

[*]E-mail: chunlei.zhu@nankai.edu.cn (C.Z.); tangbenz@cuhk.edu.cn (B.Z.T).

Experimental Section

Chemicals and Materials.

Lauric acid (LA), myristic acid (MA), palmitic acid (PA), and stearic acid (SA) were purchased from Meryer. 2-Methacryloyloxyethyl phosphorylcholine (MPC), acrylamide (AAM), *N*,*N*'-methylene bisacrylamide (MBA), tetramethylethylenediamine (TEMED), and ammonium persulfate (APS) were obtained from J&K, J&K, Fuchen, Aladdin, and Energy chemical, respectively. *n*-Butylamine, $Pd(PPh_3)_4$, and *N*-(3-aminopropyl) methacrylamide hydrochloride (APM) were purchased from Aladdin, Energy Chemical, and Heowns, respectively. Tetrahydrofuran (THF) and dimethyl sulfoxide (DMSO) were obtained from Aladdin. Dichloromethane (DCM), dimethyl formamide (DMF), ethyl acetate, petroleum ether, trimethylamine, potassium carbonate (K_2CO_3), and sodium sulphate (Na_2SO_4) were purchased from Tianjin Bohai Chemical Industry Group Co., Ltd. Tryptone soy broth (TSB) and tetracycline hydrochloride were ordered from OXOID (Basingstoke, UK) and Solarbio, respectively. Roswell Park Memorial Institute 1640 (RPMI 1640), penicillin-streptomycin solution (100×), and phosphate buffered saline (PBS, 10 mM, pH = 7.4) were ordered from Thermal Fisher Scientific. Fetal bovine serum (FBS) was obtained from Zhejiang Tianhang Biotechnology co., Ltd. Hoechst 33342 and 3-(4,5-dimethylthiazol-2-yl)-2,5-diphenyltetrazolium bromide (MTT) were purchased from Beyotime Biotechnology. All chemicals were used as received without further purification. The water used in all experiments was obtained by filtering through a set of HEAL FORCE cartridges (Smart-N15VF).

*Synthesis of compound **3**.* Compound **1** was synthesized according to a previously published paper.[1] Next, a mixture of compound **1** (1.32 g, 5 mmol), *n*-butylamine (compound **2**, 300 μL, 15 mmol), and K_2CO_3 (69 mg, 0.5 mmol) in 15 mL of ethanol was heated to reflux and stirred for 5 h. The reaction was then quenched with dilute HCl solution (0.1 M), followed by extraction with DCM three times. After solvent evaporation under reduced pressure, the crude product was purified by column chromatography on silica gel (ethyl acetate/petroleum ether =1:20, v/v) to

afford compound **3** in 45 % yield. ^{1}H-NMR (400 MHz, $CDCl_3$): δ 8.00 (d, J = 8.3 Hz, 2H), 7.53 (d, J = 8.3 Hz, 2H), 6.99 (s, 1H), 3.59 (t, J = 7.4 Hz, 2H), 2.38 (s, 3H), 1.66–1.58 (m, 2H), 1.37 (h, J = 7.3 Hz, 2H), 0.96 (t, J = 7.3 Hz, 3H). ^{13}C-NMR (100 MHz, $CDCl_3$): δ 170.64, 163.17, 139.18, 133.44, 133.22, 131.96, 125.48, 124.52, 40.50, 31.45, 20.03, 15.84, 13.70. HRMS (ESI, m/z, $C_{15}H_{17}BrN_2O$, [M + H^+]): calcd, 321.0584; found, 321.0599.

*Synthesis of compound **4**.* 4-Bromo-*N*-(4-methoxyphenyl)-*N*-phenylaniline (700 mg, 2 mmol), pinacol diborate (507 mg, 2 mmol), potassium acetate (392 mg, 4 mmol), and 1,1'-bisdiphenylphosphine ferrocene dichloride palladium (73 mg, 0.1 mmol) were placed in a round-bottom flask, which was evacuated and purged with argon gas three times. After adding 6 mL of 1,4-dioxane, the mixture was heated to 100 °C and stirred for 12 h. The product was then diluted with DCM and washed with saturated brine three times. After solvent evaporation under reduced pressure, the crude product was purified by column chromatography on silica gel (ethyl acetate/petroleum ether = 1:20, v/v) to afford compound **4** in 70 % yield. ^{1}H-NMR (400 MHz, $CDCl_3$): δ 7.63 (d, J = 6.7 Hz, 2H), 7.22 (t, J = 8 Hz, 2H), 7.11–7.04 (m, 4H), 7.02–6.94 (m, 3H), 6.84 (d, J = 8.9 Hz, 2H), 3.79 (s, 3H), 1.32 (s, 12H). ^{13}C-NMR (100 MHz, $CDCl_3$): δ 156.56, 150.95, 147.61, 140.29, 135.85, 129.24, 127.79, 124.17, 122.84, 120.49, 114.87, 83.52, 55.51, 24.91. HRMS (ESI, m/z, $C_{25}H_{28}BNO_3$, [M + Na^+]): calcd, 424.1962; found, 424.2058.

Synthesis of TICT@AIE. Compound **3** (192 mg, 0.6 mmol), compound **4** (200 mg, 0.5 mmol), $Pd(PPh_3)_4$ (58 mg, 0.05 mmol), and K_2CO_3 (690 mg, 5 mmol) were placed in a round-bottom flask, which was evacuated and purged with argon gas three times. After adding 6 mL of THF/water mixture (2:1, v/v), the system was heated to 60 °C and stirred for 12 h. The reaction was then quenched with water, followed by extraction with DCM three times. After solvent evaporation under reduced pressure, the crude product was purified by column chromatography on silica gel (ethyl acetate/petroleum ether = 1:50, v/v) to afford the target molecule (denoted as TICT@AIE) in 72.5 % yield. ^{1}H-NMR (400 MHz, $CDCl_3$): δ 8.16 (d, J = 8.1 Hz, 2H), 7.62 (d, J = 8.1 Hz, 2H),

7.49 (d, J = 8.4 Hz, 2H), 7.27 (s, 1H), 7.23 (s, 1H), 7.17–6.94 (m, 8H), 6.93–6.81 (m, 2H), 3.81 (s, 3H), 3.61 (t, J = 7.4 Hz, 2H), 2.40 (s, 1H), 1.67–1.57 (m, 2H), 1.38 (q, J = 7.5 Hz, 2H), 0.96 (t, J = 7.3 Hz, 3H). ^{13}C-NMR (100 MHz, $CDCl_3$): δ 170.79, 162.24, 156.51, 148.16, 147.76, 142.12, 140.41, 138.37, 132.96, 132.67, 129.26, 127.63, 126.95, 126.60, 123.65, 122.56, 122.21, 114.92, 55.53, 40.48, 31.51, 24.91, 20.07, 13.74. HRMS (ESI, m/z, $C_{34}H_{33}N_3O_2$, [M + H^+]): calcd, 516.2633; found, 516.2649.

Theoretical Calculation. Theoretical calculation was carried out using the Gaussian 09 software. Geometry optimization was performed using density functional theory (DFT) at B3LYP/6-31G* level of theory. The electronic distribution of the frontier molecular orbitals (FMOs) were drawn using Gaussview 5.0.9.

Preparation of TICT@AIE-doped fatty acids. The solid powders of LA (m. p. ≈ 44 °C) and LA/SA mixture (at a weight ratio of 4:1, m. p. ≈ 39 °C) were physically blended with different doping ratios of TICT@AIE (0.05 wt.%, 0.10 wt.%, 0.50 wt.%, and 1.00 wt.%), which were heated to the temperature higher than the melting point to completely dissolve TICT@AIE. After cooling to room temperature, a series of TICT@AIE-doped fatty acid solids were obtained, which were then ground into uniform powders for subsequent use. Following the identical operation, the solids of MA (m. p. ≈ 54 °C), PA (m. p. ≈ 63 °C), and SA (m. p. ≈ 69 °C) doped with 0.10 wt.% TICT@AIE were also prepared.

Temperature-dependent change in the emission of TICT@AIE-doped fatty acids. The TICT@AIE-doped fatty acid solids were melted and then dropped onto a clean glass slide. The glass slide was then placed under a 365-nm UV lamp. The changes in the emission color during the cooling process were recorded by a digital camera, and the temperature was monitored by an infrared camera (FLIR, E6).

Fabrication of nanoparticles made of TICT@AIE-doped LA/SA via in situ surface polymerization. To facilitate *in situ* surface polymerization, we first synthesized double-bond modified LA (*i.e.*, *N*-(3-methacrylamidopropyl)dodecanamide) by referring to our recently published paper.[2] The double-bond modified LA was mixed with TICT@AIE-doped LA/SA solid (doping ratio = 3.00 wt.%) at a weight ratio of 1.00 wt.%. The zwitterionic monomer MPC and initiator APS were prepared as aqueous stock solutions at the concentration of 100 mg mL^{-1}. The stock solution of the cross-linker MBA was prepared in anhydrous DMSO at a concentration of 100 mg mL^{-1}. The catalyst TEMED was prepared as 10% (v/v) aqueous solution. The final molar ratio of the TICT@AIE-doped LA/SA solid, MPC, MBA, TEMED, and APS was set at 1:600:300:30:60. Specifically, the solid fatty acid was added into hot water and ultrasonicated for 10 min to form uniform nanoparticles, which was followed by the addition of MPC, MBA, and TEMED and ultrasonication for another 2 min. Radical polymerization was then initiated on the surface of the nanoparticles by the addition of APS. The polymerization was allowed to proceed at 4 °C for 2 h, the solution of which was then dialyzed against water overnight to remove water-soluble by-products and unreacted monomers. For the convenience of discussion, the resultant nanoparticles were denoted as Poly–TICT@AIE. Since the zwitterionic MPC was able to exclude non-specific interactions with biological species, Poly–TICT@AIE was used for non-invasive biofilm imaging.

To facilitate efficient cellular uptake, the cationic form of the nanothermometer was fabricated by replacing MPC by the neutral monomer AAM and positively charged monomer APM during *in situ* surface polymerization. Specifically, AAM and APM were prepared as aqueous stock solutions at the concentration of 100 mg mL^{-1}. The final molar ratio of the TICT@AIE-doped LA/SA solid, AAM, APM, MBA, TEMED, and APS was set at 1:800:100:600:30:60. The reaction conditions and purification steps were identical to the procedure described for Poly–TICT@AIE. For the convenience of discussion, the resultant nanoparticles were denoted as Poly–TICT@AIE(+).

Characterization of TICT@AIE, TICT@AIE-doped LA/SA solid, Poly–TICT@AIE, and

Poly–TICT@AIE(+). The absorption spectra of TICT@AIE and Poly–TICT@AIE were measured by a UV–Vis spectrophotometer (Shimadzu, UV-2600). The corresponding fluorescence spectra were measured on a fluorometer (HITACHI, F-4700). In addition, the fluorescence spectra at different temperatures were measured on a fluorometer (HITACHI, F-4700), which was attached to a circulating bath (cooling and heating) for temperature control. The corresponding errors represented standard deviation, which was derived from the spectra by three consecutive measurements at a fixed temperature. The morphology of Poly–TICT@AIE was characterized by transmission electron microscopy (TEM, FEI, Talos F200X G2). The particle size distributions of Poly–TICT@AIE and Poly–TICT@AIE(+) as well as the zeta potential of Poly–TICT@AIE(+) were measured by dynamic light scattering (DLS, Malvern, Zetasizer Nano ZS90). Differential scanning calorimetry (DSC, NETZSCH, DSC204) was used to test the thermal properties of LA/SA and TICT@AIE-doped LA/SA solid (doping ratio = 3.00 wt.%), in which the samples (5–10 mg) were heated from 0 °C to 95 °C at a heating rate of 5 °C per min in a nitrogen atmosphere with a purge flow of 50 mL min^{-1}. The concentration of TICT@AIE was determined by measuring the UV–Vis spectra of disassembled Poly–TICT@AIE and Poly–TICT@AIE(+) (dissolved in ethanol and ultrasonicated for 10 min), followed by quantification using the corresponding calibration curve. Encapsulation efficiency (EE) and loading content (LC) were then calculated using equations (1) and (2), respectively.

EE = (weight of the payload in nanoparticles)/(weight of the added payload) × 100% (1)

LC = (weight of the payload in nanoparticles)/(weight of the nanoparticles) × 100% (2)

Evaluation of the fluorescence properties of Poly–TICT@AIE and Poly–TICT@AIE(+) under different conditions. The nanoparticles (0.5 mg mL^{-1}) were mixed with potassium chloride under different concentrations (50, 100, 200, 300, 400, and 500 mM), at different pH values (3.0, 4.0, 5.0, 6.0, 7.0, 7.4, 8.0, 9.0, 10.0, and 11.0), and in different media (water, PBS, RPMI 1640, and RPMI 1640 + 10% FBS) (v/v = 1:1). All samples were equilibrated at 25 °C for 10 min prior to the measurement of the emission spectra (Ex = 405 nm for Poly–TICT@AIE; Ex = 470 nm for

Poly–TICT@AIE(+)). The fluorescence intensity at 590 nm (emission maximum) was used for quantitative analysis.

Fluorescence lifetime of Poly–TICT@AIE. The fluorescence lifetime decay curves of Poly–TICT@AIE at different temperatures were measured on a fluorescence spectrometer (Edinburgh, FLS1000), which were fitted by a double-exponential function as follows:

$$I(t) = I_0 [A_1 \exp(-t/\tau_1) + A_2 \exp(-t/\tau_2)] \quad (3)$$

Further, the fluorescence lifetime (τ) was determined by the following equation:

$$\tau = (A_1 \tau_1^2 + A_2 \tau_2^2) / (A_1 \tau_1 + A_2 \tau_2) \quad (4)$$

where I is the fluorescence intensity; τ is the average fluorescence lifetime; t is the time of fluorescence decay; τ_1 is the fluorescence lifetime of the long component; τ_2 is the fluorescence lifetime of the short component; A_1 and A_2 are the contribution of the τ_1 and τ_2, respectively.

Bacterial culture and biofilm formation. The methicillin-resistant *Staphylococcus aureus* (MRSA) were provided by Prof. Jianfeng Liu (Institute of Radiation Medicine, Chinese Academy of Medical Sciences and Peking Union Medical College). For the culture of MRSA, a single colony of MRSA on a solid Tryptic Soy Broth (TSB) agar plate was transferred to 5 mL of TSB broth medium with 10 μg mL^{-1} tetracycline hydrochloride in a shaking incubator (170 rpm) at 37 °C overnight. The bacterial cells were harvested by centrifugation (3500 *g* for 5 min) and washed with phosphate buffer saline (PBS, pH = 7.4) three times. The supernatant was discarded and the remaining MRSA was resuspended in PBS, which was diluted to an optical density of 1.0 at 600 nm (OD_{600} = 1.0). For the culture of MRSA biofilms, a bacterial suspension (PBS, 1.5 mL) was placed in a 35-mm petri dish for 2 h at 37 °C to allow bacterial adhesion, followed by gently washing with PBS three times to remove non-adherent bacteria. The TSB medium was added and then incubated at 37 °C for 24 h. Such operation was repeated two times to allow the formation of bacterial biofilms after 72 h of incubation.

Fluorescence imaging of MRSA biofilms at different temperatures. MRSA biofilms were carefully washed with PBS and incubated with Poly–TICT@AIE (0.5 mg mL^{-1}) at 37 °C for 30 min. Non-infiltrated nanoparticles were removed by gently washing with PBS. Next, the biofilms incubated at different temperatures were subjected to 3D imaging using the z-axis scanning mode of a CLSM (Nikon, $A1^{+}$; Ex = 405 nm, Em = 510–550 nm for the green channel and 570–610 nm for the red channel). To demonstrate the infiltrated Poly–TICT@AIE was not ingested by the residing bacteria, the biofilms were stained by a fluorescent indicator for bacteria (SYTO 9, 3.34 μM). After removing the unbound dye molecules by gently washing with PBS, the biofilms were subjected to 3D imaging using the z-axis scanning mode of CLSM (SYTO 9, Ex = 488 nm, Em = 490–530 nm; Poly–TICT@AIE, Ex = 405 nm, Em = 530–630 nm). The temperature for all experiments was calibrated by an infrared camera (FLIR, E6).

Fluorescence lifetime imaging of MRSA biofilms at different temperatures. MRSA biofilms were treated the same way as described in "*Fluorescence imaging of MRSA biofilms at different temperatures.*" Fluorescence lifetime imaging of MRSA biofilms at different temperatures was performed on a time-resolved CLSM with single-molecule sensitivity (PicoQuant, Microtime 200), in which a 375-nm laser was used as the excitation wavelength for fluorescence lifetime imaging. The fluorescence lifetime was derived from the collected fluorescence decay curves. The temperature for all experiments was calibrated by an infrared camera (FLIR, E6).

Calculation of the relative thermal sensitivity (S_r) and temperature resolution (δT) of Poly–TICT@AIE for temperature sensing. The relative thermal sensitivity (S_r) is defined as:

$$\text{Spectral position:} \quad S_r^{\lambda} = \frac{1}{\lambda}\left|\frac{\partial \lambda}{\partial T}\right| \tag{5}$$

$$\text{Integral area:} \quad S_r^{I} = \frac{1}{I}\left|\frac{\partial I}{\partial T}\right| \tag{6}$$

$$\text{Fluorescence lifetime:} \quad S_r^{\tau} = \frac{1}{\tau}\left|\frac{\partial \tau}{\partial T}\right| \tag{7}$$

where S_r was presented as percent change per degree Celsius (*i.e.*, % $°C^{-1}$).

The temperature uncertainty or temperature resolution (δT) is defined as:

$$\text{Spectral position:} \quad \delta T = \frac{1}{S_r^{\lambda}} \frac{\delta \lambda}{\lambda} \tag{8}$$

$$\text{Integral area:} \quad \delta T = \frac{1}{S_r^{I}} \frac{\delta I}{I} \tag{9}$$

$$\text{Fluorescence lifetime:} \quad \delta T = \frac{1}{S_r^{\tau}} \frac{\delta \tau}{\tau} \tag{10}$$

where δT was expressed as degree Celsius (*i.e.*, °C).

Cell culture. A549 cells, a human lung adenocarcinoma epithelial cell line, were cultured in RPMI-1640 containing 10% fetal bovine serum (FBS) and 1% antibiotics (100 units/mL penicillin and 100 g/mL streptomycin) in a 5% CO_2 humidity incubator at 37 °C. The culture medium was changed every other day.

Cell viability assay. The cell viability of A549 cells incubated with different concentrations of Poly–TICT@AIE(+) was measured by the MTT assay. Specifically, A549 cells were seeded in a 96-well plate at a density of 8000–10000 cells per well and cultured overnight. Next, Poly–TICT@AIE(+) with varying concentrations of TICT@AIE (5, 10, 20, 30, 40, and 50 μM) were added into the cells, followed by incubation at 37 °C for 12 h. The cells were replenished with fresh culture medium and incubated for another 12 h. Subsequently, the MTT solution (0.5 mg mL^{-1} in medium, 100 μL per well) was added to each well and incubated at 37 °C for 4 h. After removing the MTT solution, DMSO (150 μL per well) was added to dissolve the formed formazan crystals. The absorbance values at 490 nm was recorded by a microplate reader (Tecan, Infinite M Nano). The cell viability was defined as the percentage of surviving cells versus untreated cells (n = 3 for each group).

Cellular uptake of Poly–TICT@AIE(+). A549 cells were seeded in 35-mm petri dishes at a density of 3–4 × 10^5 cells and cultured in a 5% CO_2 humidity incubator at 37 °C overnight. As for one-photon imaging, the cells were incubated with Poly–TICT@AIE(+) ([TICT@AIE] = 10 μM) at

37 °C for 1.5 h. After washing with PBS, the cells were stained by Hoechst 33342 (10 μg mL^{-1}) in RPMI-1640 at 37 °C for 10 min. Next, the medium was washed with PBS and the cells were supplemented with fresh culture medium for CLSM imaging (Nikon, $A1^{+}$). As for two-photon imaging, the cells were incubated with Poly−TICT@AIE(+) ([TICT@AIE] = 10 μM) at 37 °C for 1.5 h. After washing with PBS, the cells were supplemented with fresh culture medium for two-photon imaging (Olympus, FV1200 MPE).

Reference

(1) Huang, G.-J.; Yang, J.-S. The *N*-Arylamino Conjugation Effect in the Photochemistry of Fluorescent Protein Chromophores and Aminostilbenes. *Chem. Asian J.* **2010**, *5*, 2075−2085.

(2) Xue, K.; Yang, C.; Wang, C.; Liu, Y.; Liu, J.; Shi, L.; Zhu, C. An Exceptional Broad-Spectrum Nanobiocide for Multimodal and Synergistic Inactivation of Drug-Resistant Bacteria. *CCS Chem.* **2021**, *3*, 531−544.

(3) Meng, L.; Jiang, S.; Song, M.; Yan, F.; Zhang, W.; Xu, B.; Tian, W. TICT-Based Near-Infrared Ratiometric Organic Fluorescent. *ACS Appl. Mater. Interfaces* **2020**, *12*, 26842−26851.

(4) Shen, Y.; Santos, H. D. A.; Ximendes, E. C.; Lifante, J.; Sanz-Portilla, A.; Monge, L.; Fernández, N.; Chaves-Coira, I.; Jacinto, C.; Brites, C. D. S.; Carlos, L. D.; Benayas, A.; Iglesias-de la Cruz, M. C.; Jaque, D. Ag_2S Nanoheaters with Multiparameter Sensing for Reliable Thermal Feedback during in Vivo Tumor Therapy. *Adv. Funct. Mater.* **2020**, *30*, 2002730.

(5) Bolek, P.; Zeler, J.; Brites, C. D. S.; Trojan-Piegza, J.; Carlos, L. D.; Zych, E. Ga-Modified YAG:Pr^{3+} Dual-Mode Tunable Luminescence Thermometers. *Chem. Eng. J.* **2021**, *421*, 129764.

(6) Marciniak, L.; Bednarkiewicz, A.; Hreniak, D.; Strek, W. The Influence of Nd^{3+} Concentration and Alkali Ions on the Sensitivity of Non-Contact Temperature Measurements in $ALaP_4O_{12}$:Nd^{3+} (A = Li, K, Na, Rb) Nanocrystalline Luminescent Thermometers. *J. Mater. Chem. C* **2016**, *4*, 11284–11290.

(7) Xu, M.; Zou, X.; Su, Q.; Yuan, W.; Cao, C.; Wang, Q.; Zhu, X.; Feng, W., Li, F. Ratiometric Nanothermometer in Vivo Based on Triplet Sensitized Upconversion. *Nat. Commun.* **2018**, *9*, 2698.

(8) Tanimoto, R., Hiraiwa, T., Nakai, Y. Shindo, Y.; Oka, K.; Hiroi, N.; Funahashi, A. Detection of Temperature Difference in Neuronal Cells. *Sci. Rep.* **2016**, *6*, 22071.

(9) Shang, L.; Stockmar, F.; Azadfar, N.; Nienhaus, G. U. Intracellular Thermometry by Using Fluorescent Gold Nanoclusters. *Angew. Chem. Int. Ed.* **2013**, *52*, 11154–11157.

(10) Savchuk, O. A.; Silvestre, O. F.; Adão, R. M. R.; Nieder, J. B. GFP Fluorescence Peak Fraction Analysis Based Nanothermometer for the Assessment of Exothermal Mitochondria Activity in Live Cells. *Sci. Rep.* **2019**, *9*, 7535.

(11) Nakano, M.; Arai, Y.; Kotera, I.; Okabe, K.; Kamei, Y.; Nagai, T. Genetically Encoded Ratiometric Fluorescent Thermometer with Wide Range and Rapid Response. *PLoS One* **2017**, *12*, e0172344.

(12) Arai, S.; Lee, S.-C.; Zhai, D.; Suzuki, M.; Chang, Y. T. A Molecular Fluorescent Probe for Targeted Visualization of Temperature at the Endoplasmic Reticulum. *Sci. Rep.* **2014**, *4*, 6701.

(13) Arai, S.; Suzuki, M.; Park, S.-J.; Yoo, J. S.; Wang, L.; Kang, N.-Y.; Ha, H.-H.; Chang, Y.-T. Mitochondria-targeted Fluorescent Thermometer Monitors Intracellular Temperature Gradient. *Chem. Commun.* **2015**, *51*, 8044–8047.

(14) Homma, M.; Takei, Y.; Murata, A.; Inoue, T.; Takeoka, S. A Ratiometric Fluorescent Molecular Probe for Visualization of Mitochondrial Temperature in Living Cells. *Chem. Commun.* **2015**, *51*, 6194–6197.

(15) Gota, C.; Kohki Okabe, K.; Funatsu, T.; Harada, Y.; Uchiyama, S. Hydrophilic Fluorescent Nanogel Thermometer for Intracellular Thermometry. *J. Am. Chem. Soc.* **2009**, *131*, 2766–2767.

(16) Uchiyama, S.; Tsuji, T.; Kawamoto, K.; Okano, K.; Fukatsu, E.; Noro, T.; Ikado, K.; Yamada, S.; Shibata, Y.; Hayashi, T.; Inada, N.; Kato, M.; Koizumi, H.; Tokuyama, H. A Cell-Targeted

Non-Cytotoxic Fluorescent Nanogel Thermometer Created with an Imidazolium-Containing Cationic Radical Initiator. *Angew. Chem. Int. Ed.* **2018**, *57*, 5413–5417.

(17) Okabe, K.; Inada, N.; Gota, C.; Harada, Y.; Funatsu, T.; Uchiyama, S. Intracellular Temperature Mapping with a Fluorescent Polymeric Thermometer and Fluorescence Lifetime Imaging Microscopy. *Nat. Commun.* **2012**, *3*, 705.

(18) Inada, N.; Fukuda, N.; Hayashi, T.; Uchiyama, S. Temperature Imaging Using a Cationic Linear Fluorescent Polymeric Thermometer and Fluorescence Lifetime Imaging Microscopy. *Nat. Protoc.* **2019**, *14*, 1293–1321.

(19) Uchiyama, S.; Tsuji, T.; Ikado, K.; Yoshida, A.; Kawamoto, K.; Hayashic, T.; Inada, N. A Cationic Fluorescent Polymeric Thermometer for the Ratiometric Sensing of Intracellular Temperature. *Analyst* **2015**, *140*, 4498–4506.

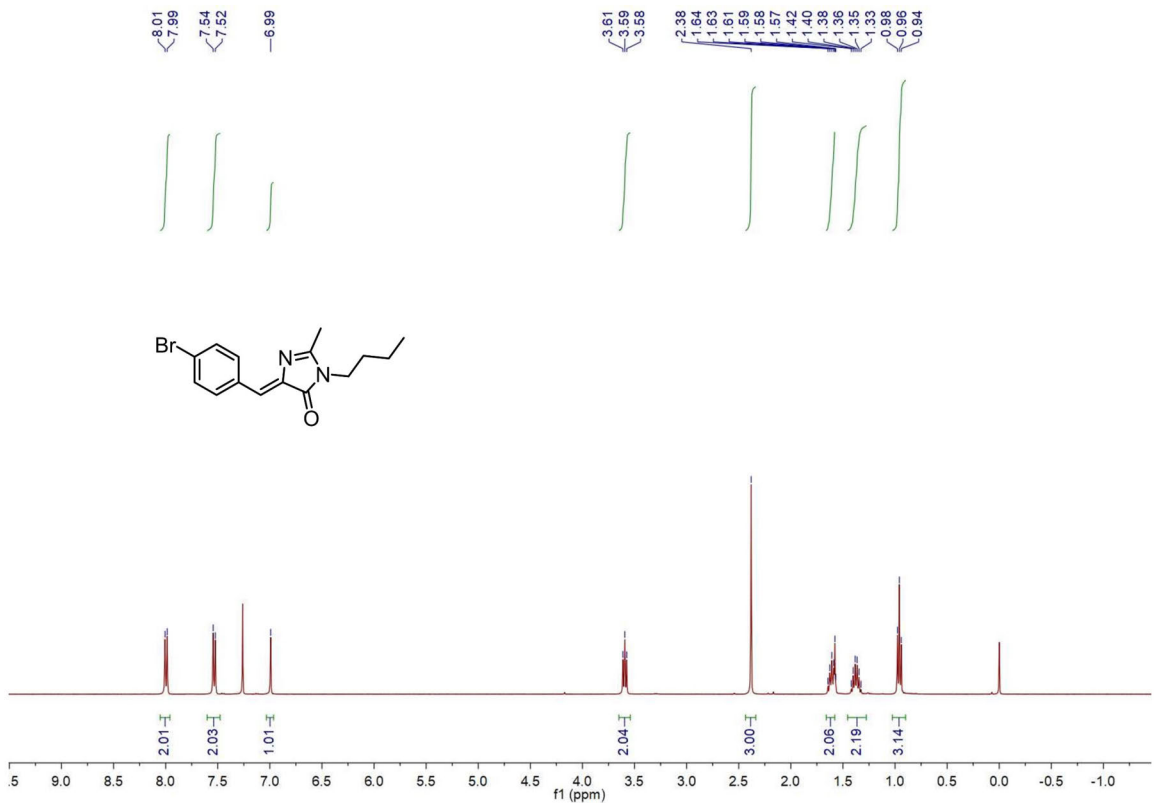

Figure S1. ^{1}H-NMR spectrum of compound **3** in $CDCl_3$.

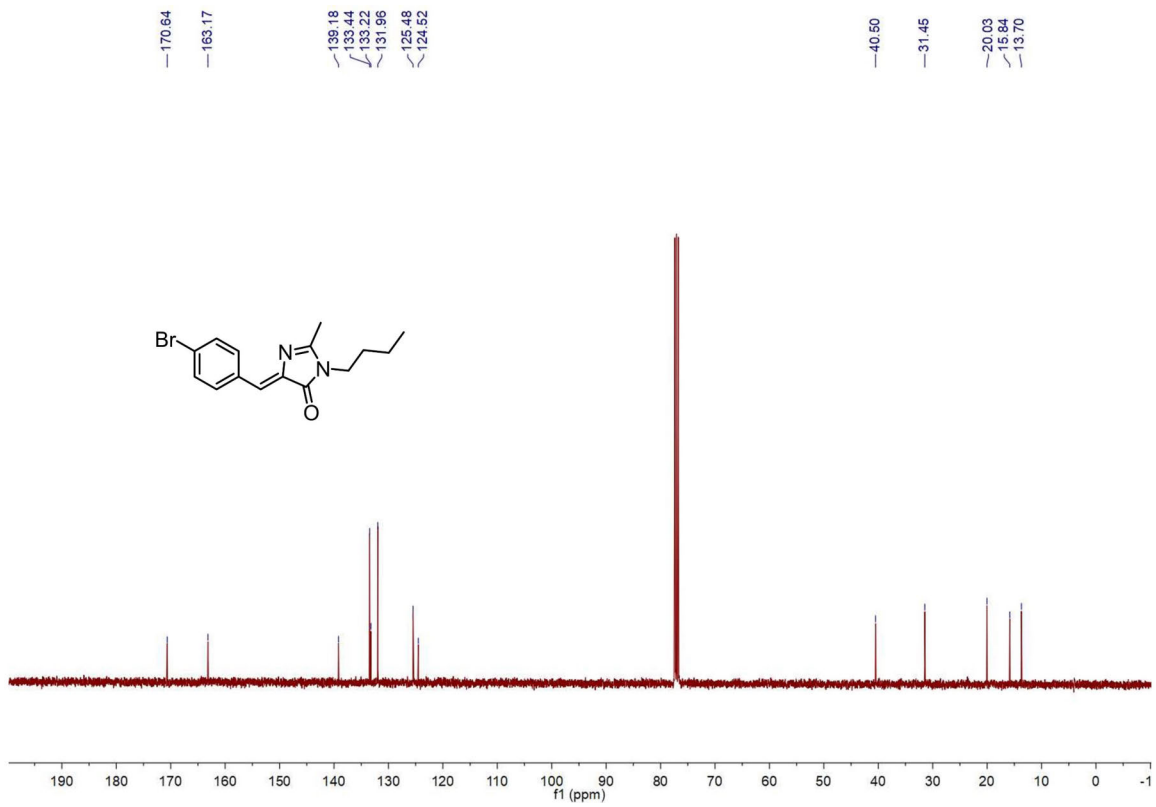

Figure S2. ^{13}C-NMR spectrum of compound **3** in $CDCl_3$.

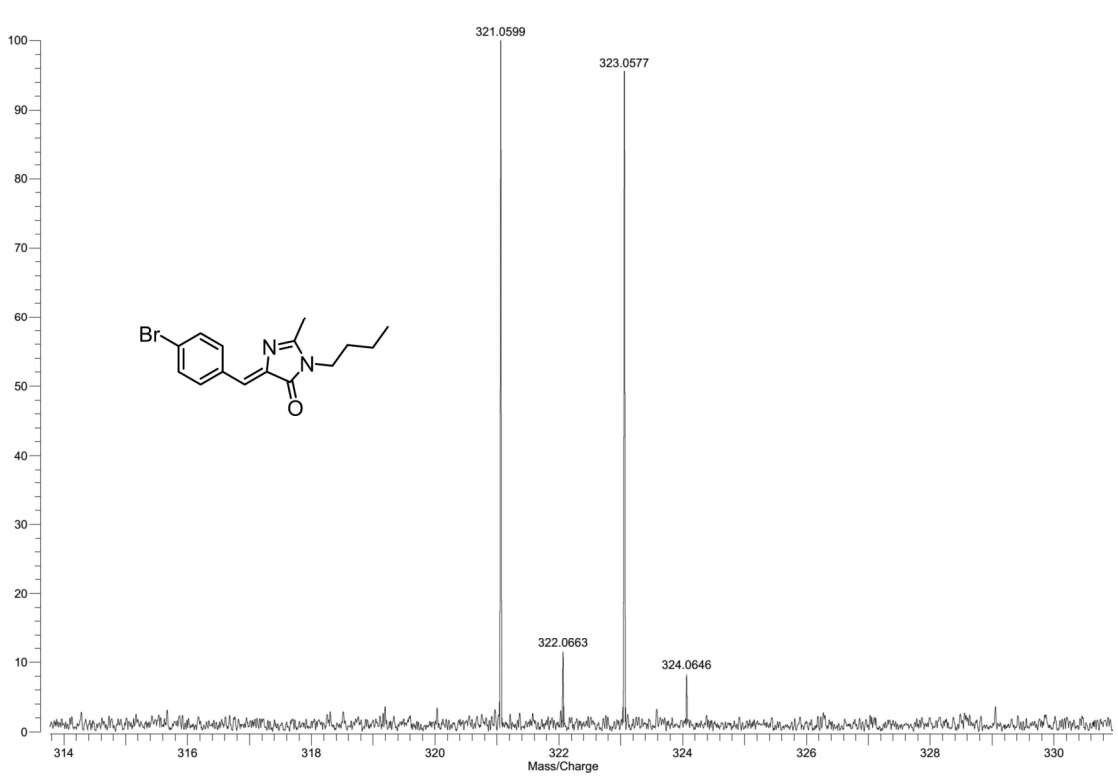

Figure S3. HRMS spectrum of compound **3**.

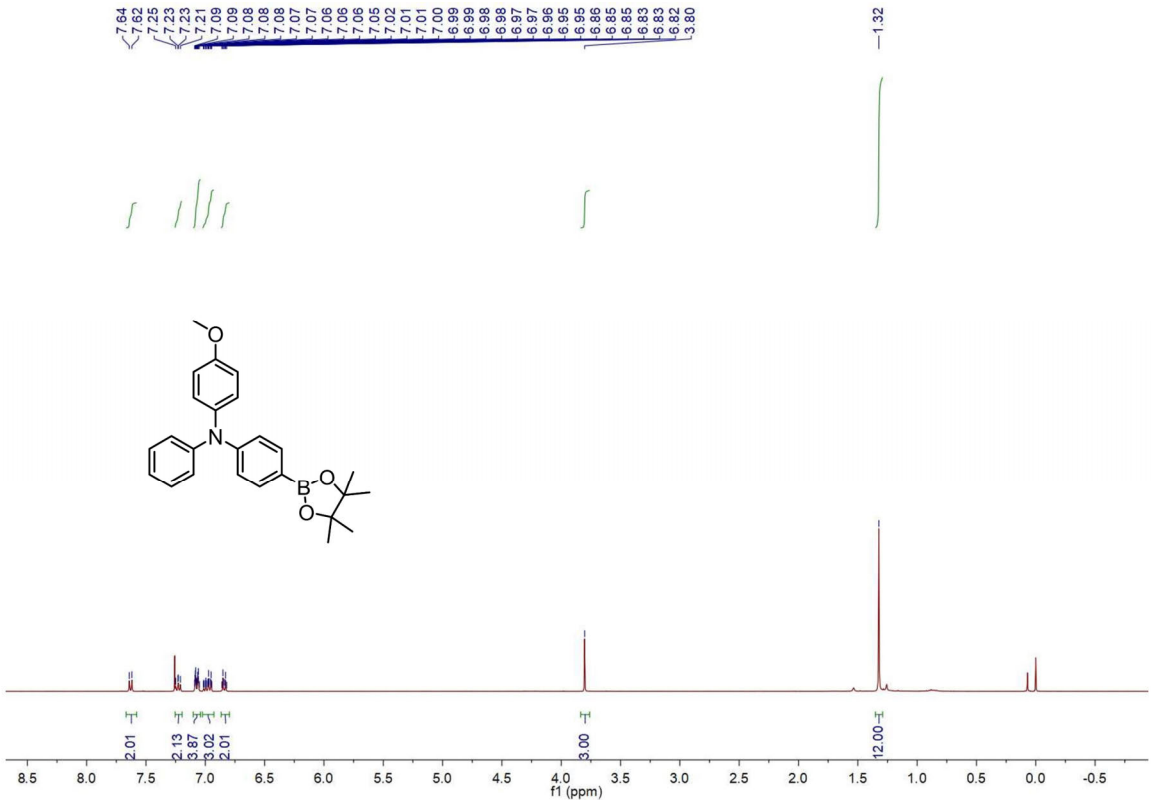

Figure S4. ^{1}H-NMR spectrum of compound **4** in $CDCl_3$.

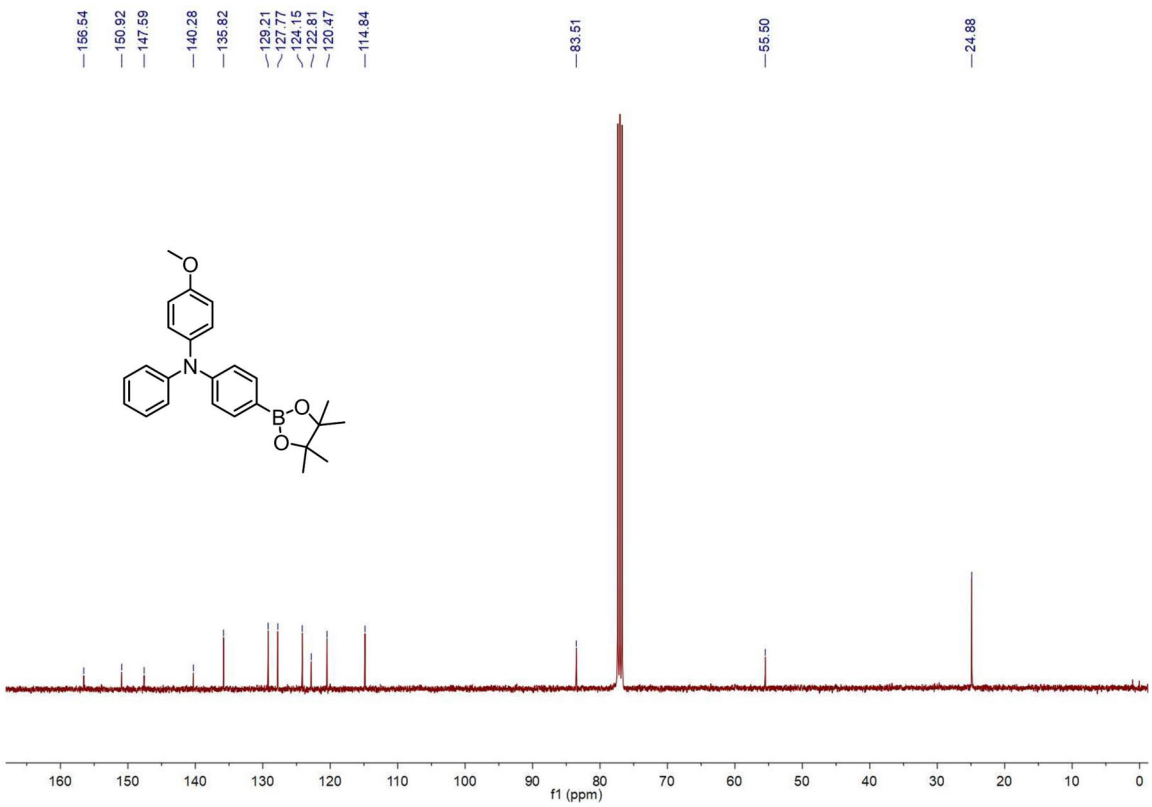

Figure S5. ^{13}C-NMR spectrum of compound **4** in $CDCl_3$.

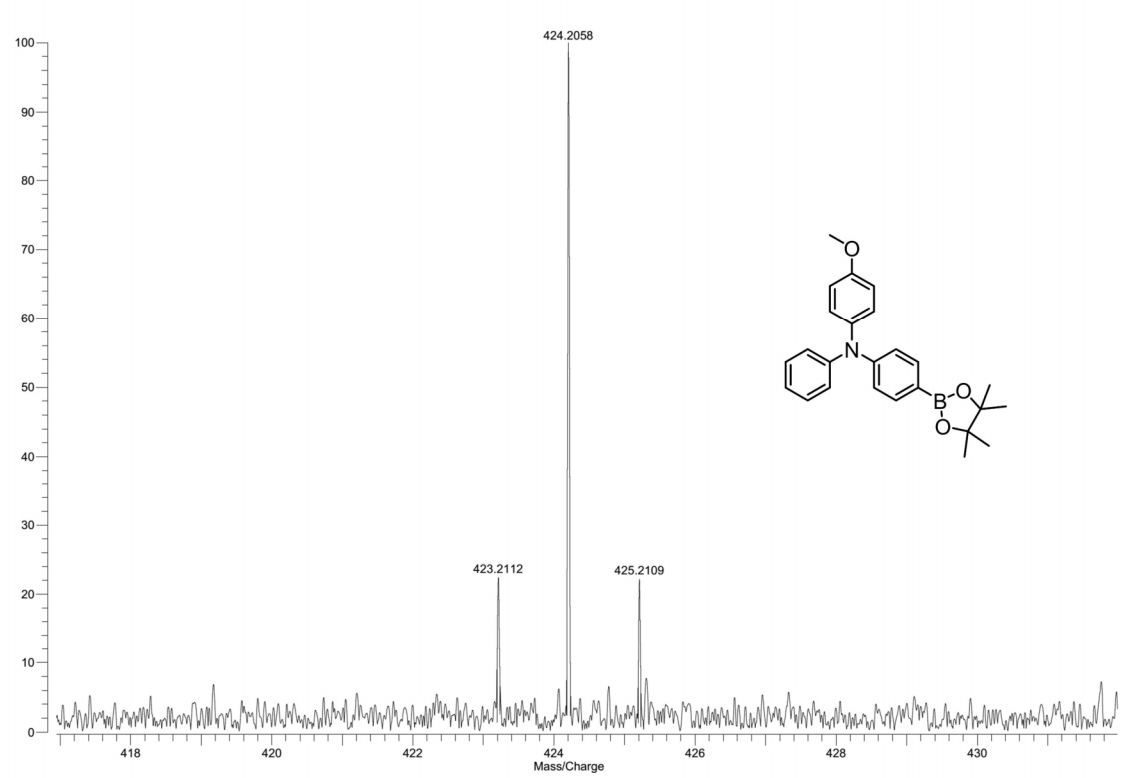

Figure S6. HRMS spectrum of compound **4**.

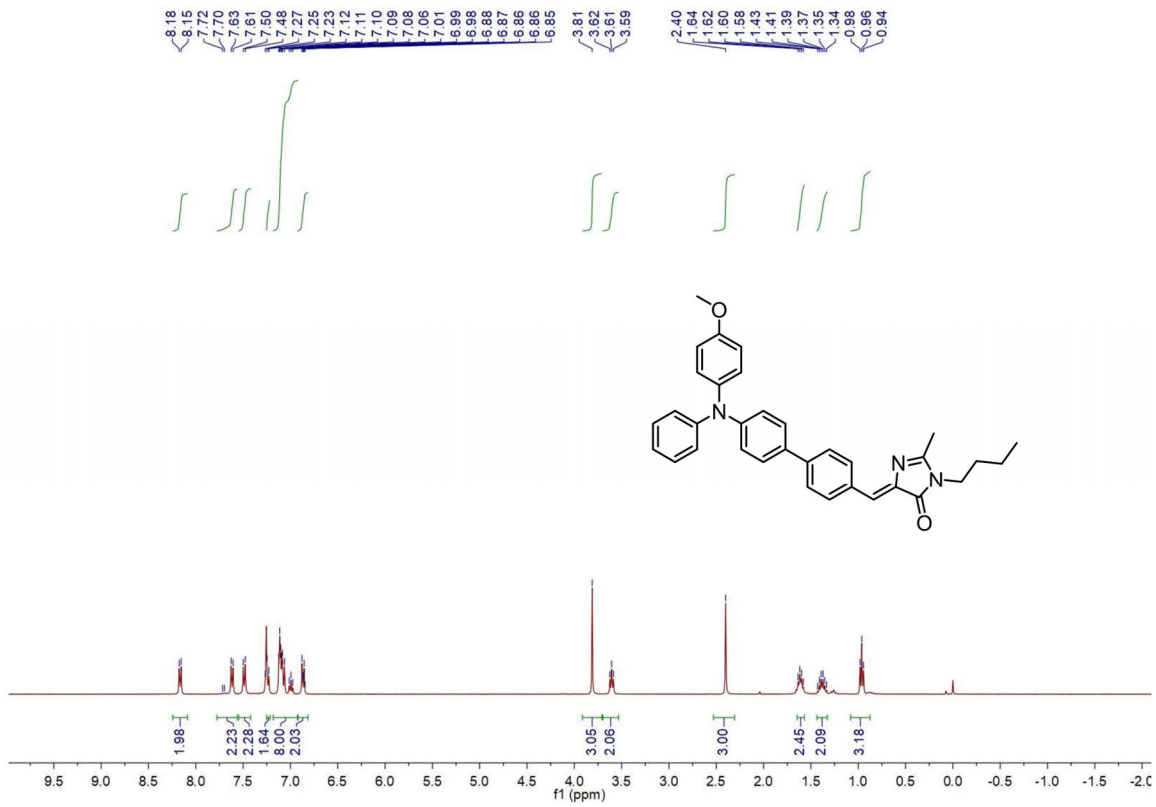

Figure S7. ^{1}H-NMR spectrum of TICT@AIE in $CDCl_3$.

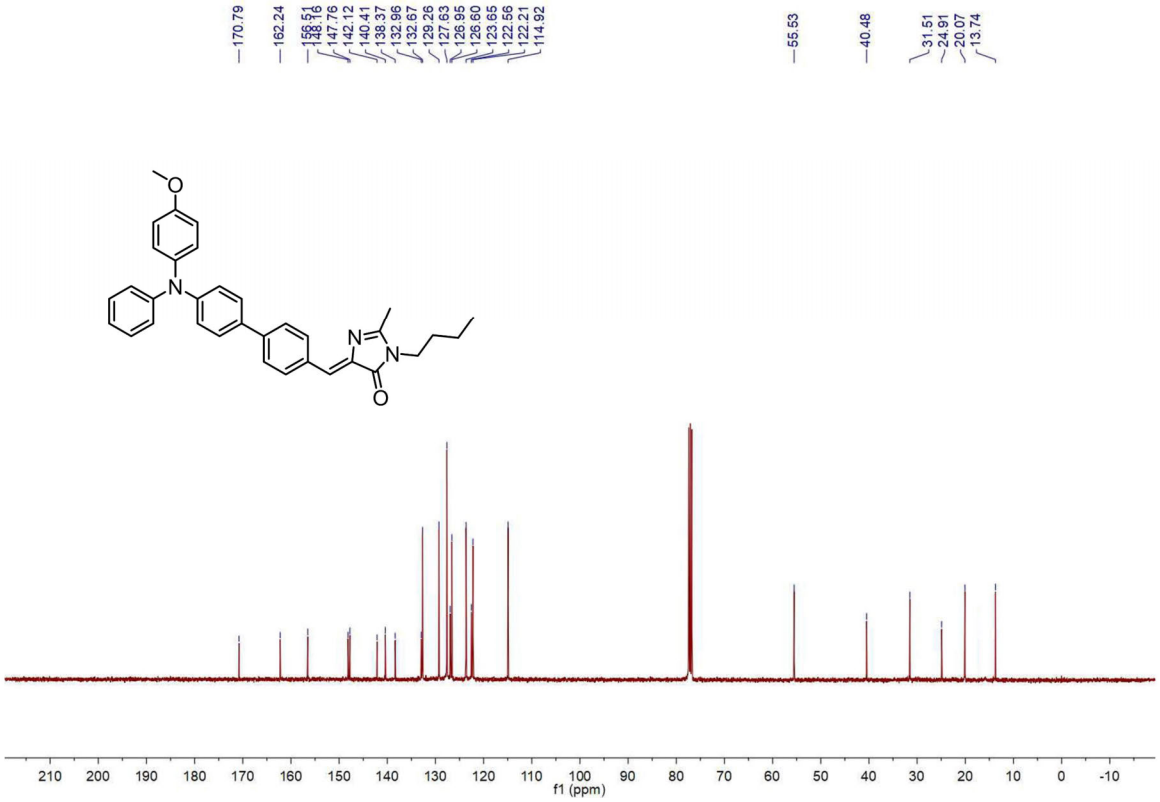

Figure S8. ^{13}C-NMR spectrum of TICT@AIE in $CDCl_3$.

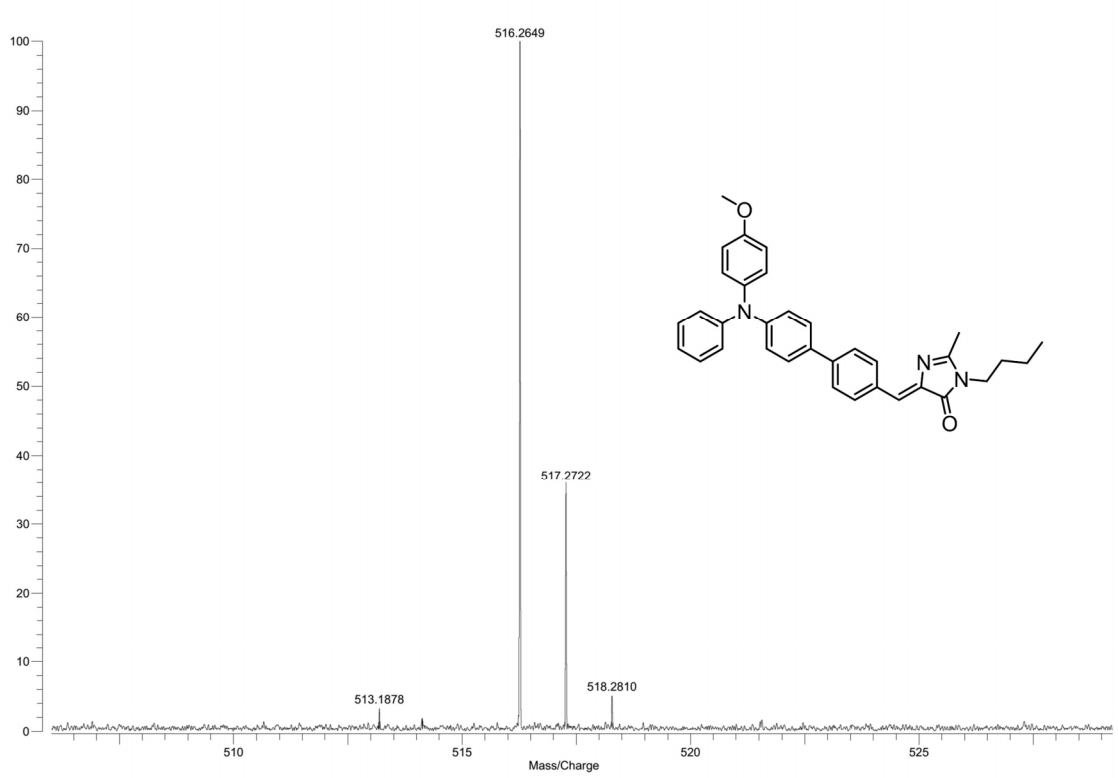

Figure S9. HRMS spectrum of TICT@AIE.

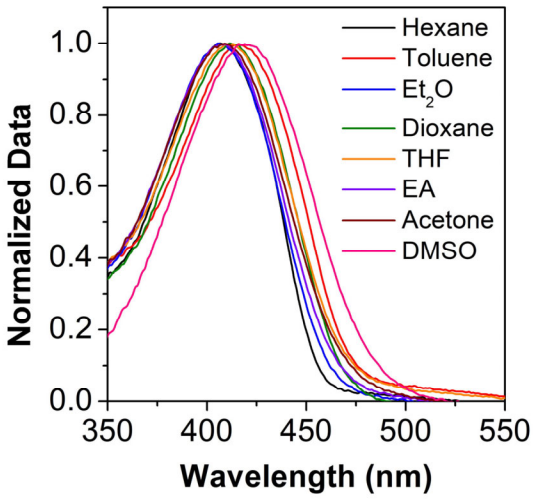

Figure S10. Normalized absorption spectra of TICT@AIE in different organic solvents.

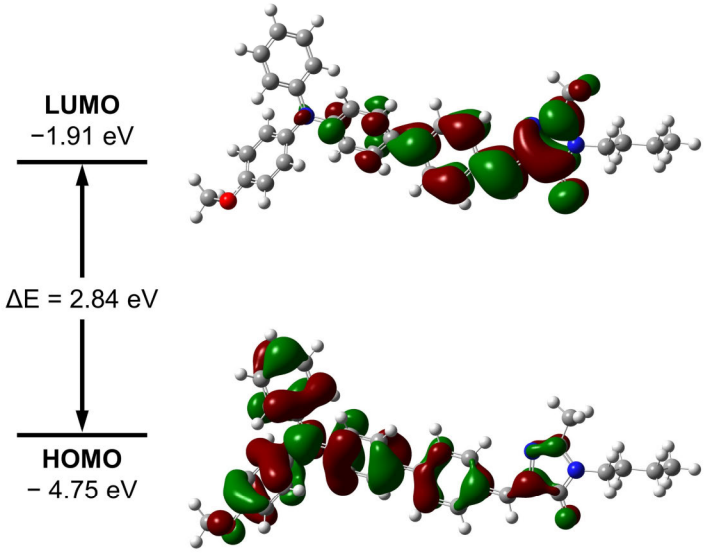

Figure S11. Calculated FMOs and corresponding energies of TICT@AIE.

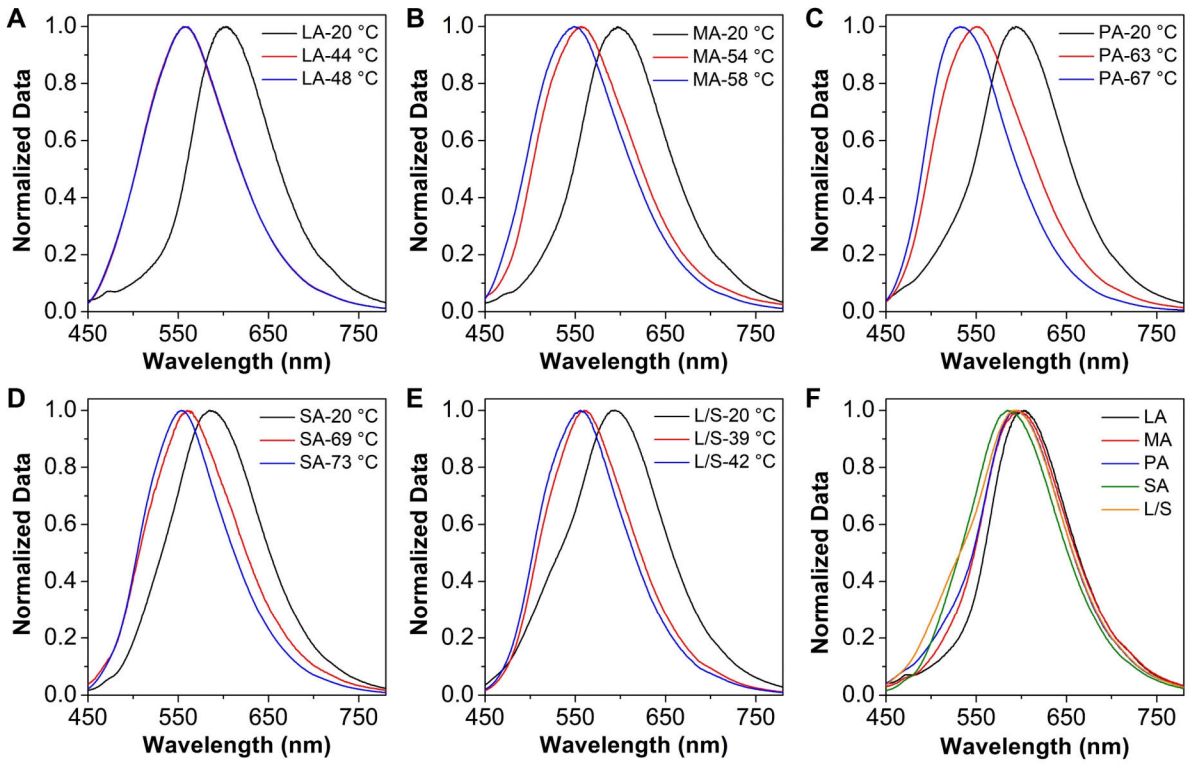

Figure S12. Emission spectra of various saturated fatty acid doped with TICT@AIE (0.10 wt.%) at different temperatures. A) LA at 20 °C, 44 °C, and 48 °C. B) MA at 20 °C, 54 °C, and 58 °C. C) PA at 20 °C, 63 °C, and 67 °C. D) SA at 20 °C, 69 °C, and 73 °C. E) LA/SA (L/S) mixture at 20 °C, 39 °C, and 42 °C. F) LA, MA, PA, SA, and LA/SA (L/S) mixture at 20 °C. Ex = 405 nm.

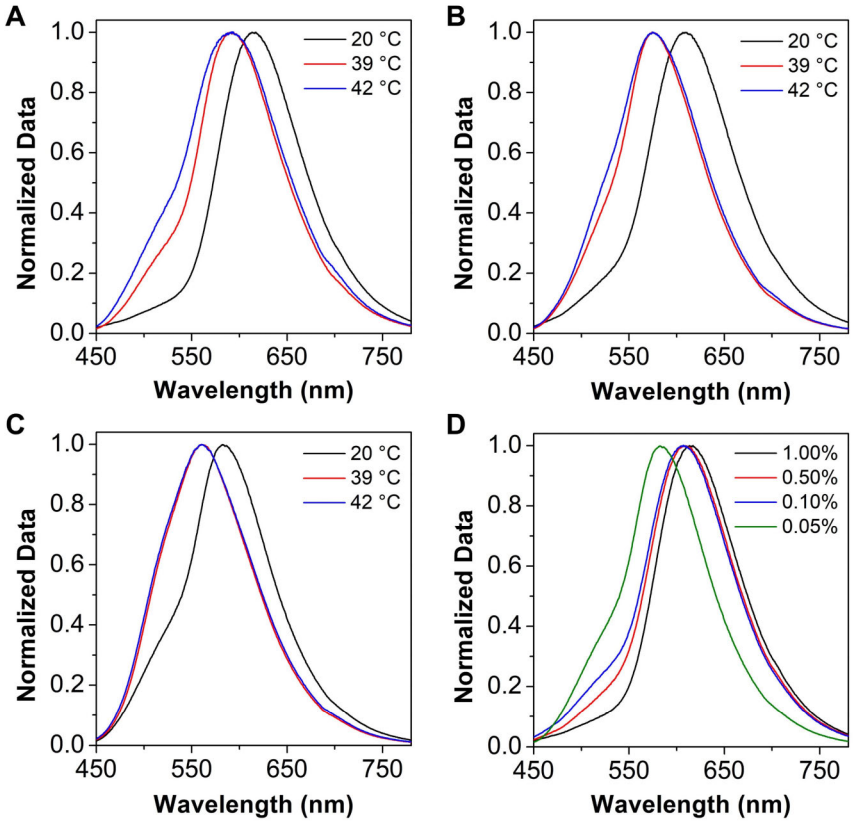

Figure S13. Emission spectra of LA/SA solids doped with different weight ratios of TICT@AIE at different temperatures. A) 1.00 wt.%, B) 0.50 wt.%, and C) 0.05 wt.% at 20 °C, 39 °C, and 42 °C. D) 1.00 wt.%, 0.50 wt.%, 0.10 wt.%, and 0.05 wt.% at 20 °C. Ex = 405 nm.

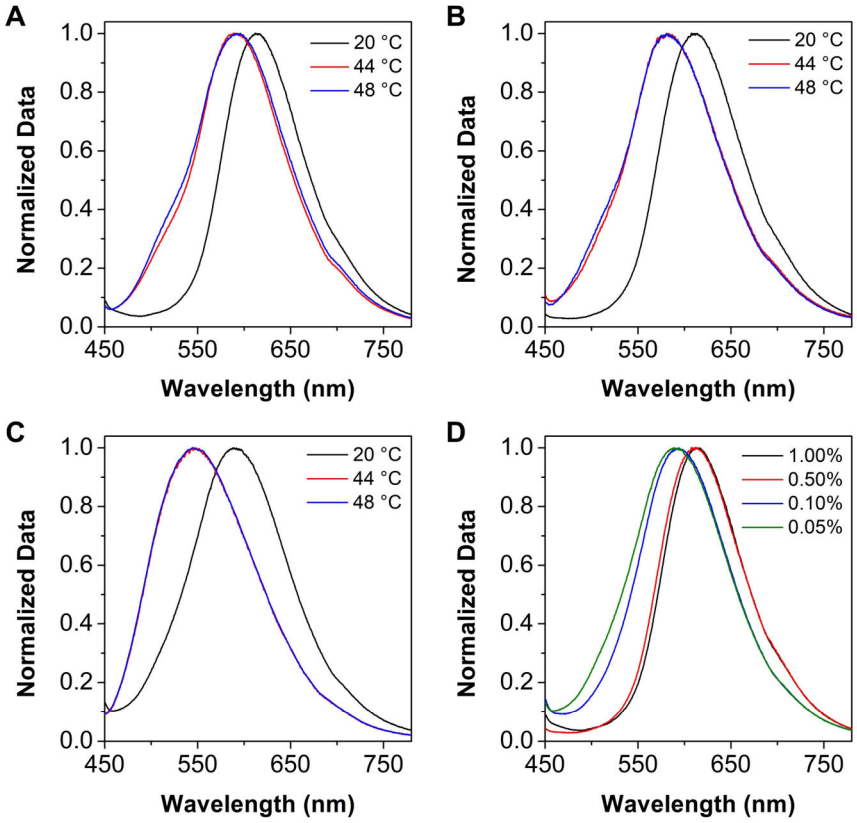

Figure S14. Emission spectra of LA doped with different weight ratios of TICT@AIE at different temperatures. A) 1.00 wt.%, B) 0.50 wt.%, and C) 0.05 wt.% at 20 °C, 44 °C, and 48 °C. D) 1.00 wt.%, 0.50 wt.%, 0.10 wt.%, and 0.05 wt.% at 20 °C. Ex = 405 nm.

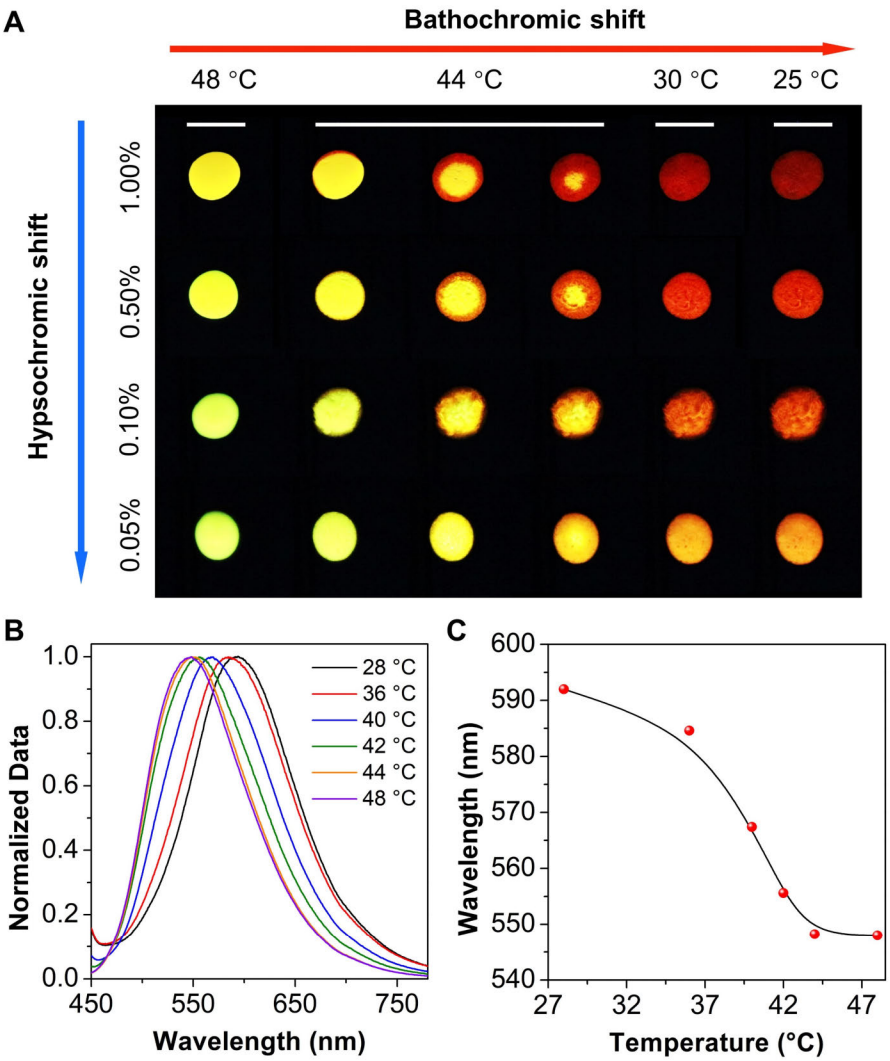

Figure S15. Temperature-dependent change in the emission of TICT@AIE-doped LA. A) A photograph taken under a 365-nm UV lamp showing the cooling process of preheated LA with different weight ratios of TICT@AIE. B) Temperature-dependent emission spectra of LA doped with 0.10 wt.% TICT@AIE. Ex = 405 nm. C) A plot of the emission maximum as a function of temperature.

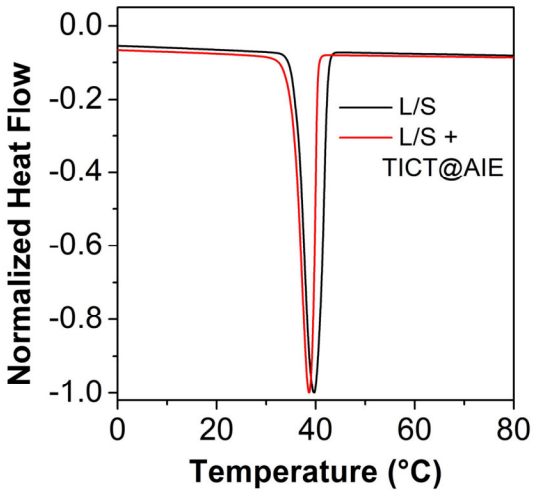

Figure S16. DSC curves of LA/SA (L/S) and LA/SA doped with 3.00 wt.% TICT@AIE (L/S + TICT@AIE).

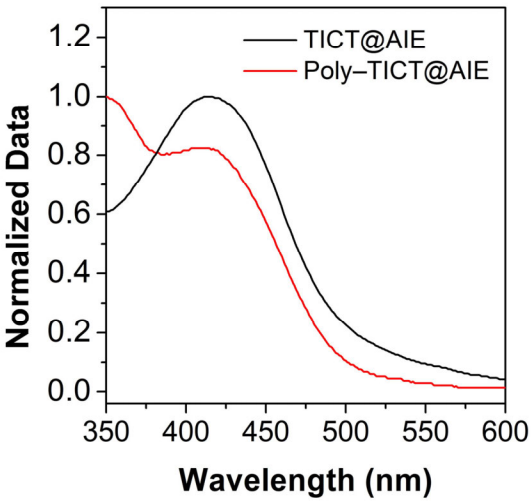

Figure S17. Normalized absorption spectra of TICT@AIE and Poly–TICT@AIE.

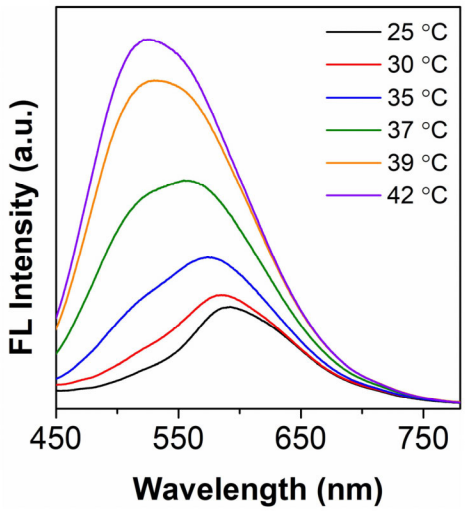

Figure S18. Emission spectra of Poly–TICT@AIE at different temperatures. Ex = 405 nm.

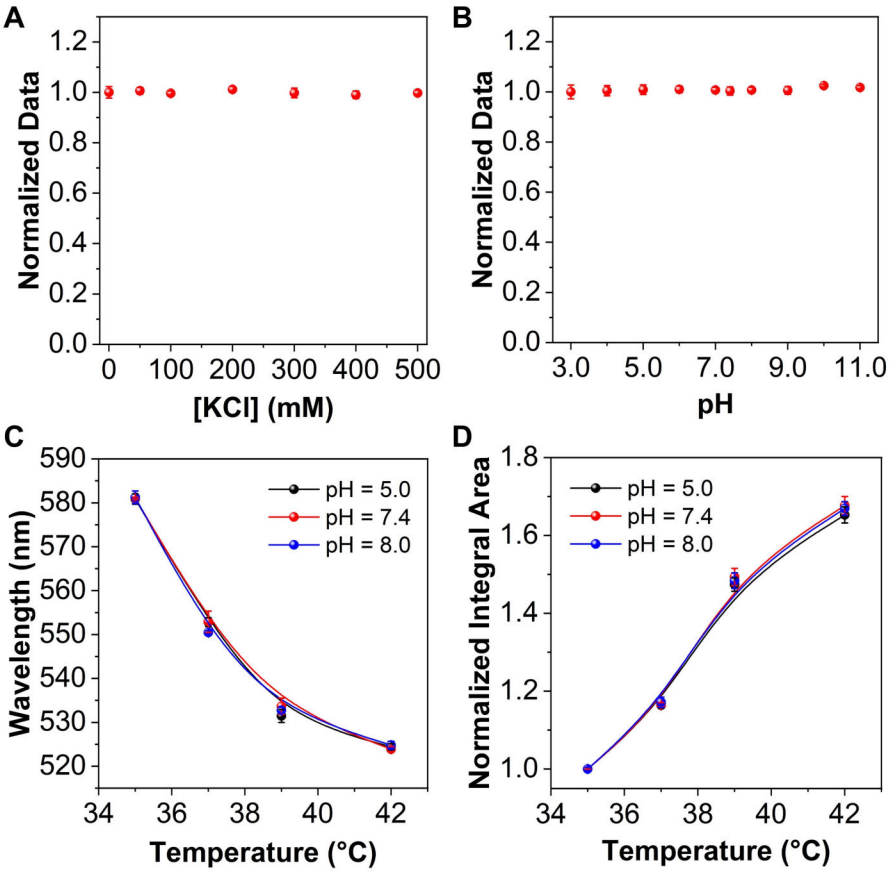

Figure S19. The impacts of ionic strength and pH values on the fluorescence intensity of Poly–TICT@AIE. A) The normalized fluorescence intensity of Poly–TICT@AIE at 590 nm in the presence of different concentrations of KCl at 25 °C. B) The normalized fluorescence intensity of Poly–TICT@AIE at 590 nm under different pH values at 25 °C. C) The plots of the emission maximum of Poly–TICT@AIE as a function of temperature between 35–42 °C under different pH values. D) The plots of the normalized integral area on the emission spectra of Poly–TICT@AIE as a function of temperature between 35–42 °C under different pH values. Ex = 405 nm.

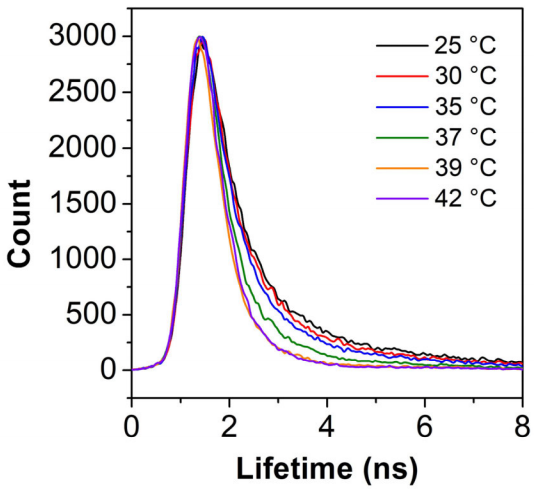

Figure S20. Fluorescence decay curves of Poly–TICT@AIE at different temperatures.

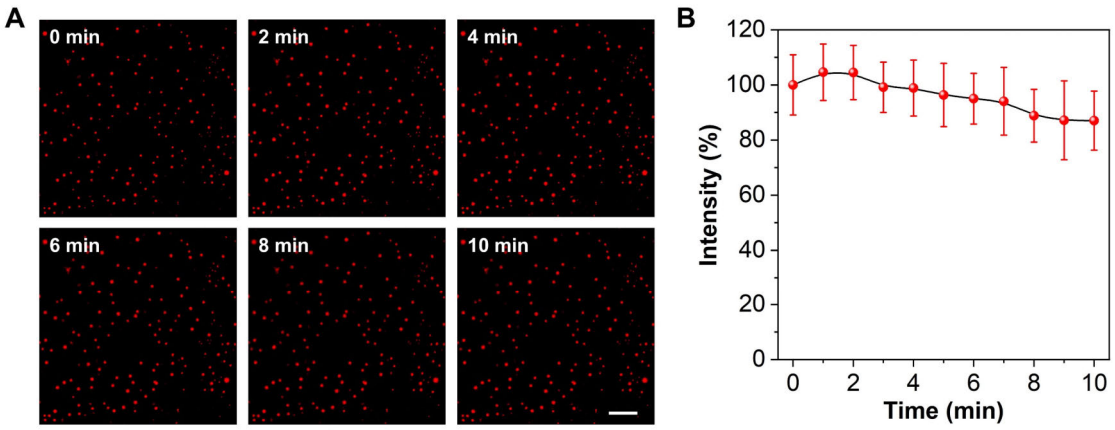

Figure S21. Photostability of Poly–TICT@AIE upon continuous excitation by a 405-nm laser for 10 min (laser power = 6%). A) CLSM images of Poly–TICT@AIE taken at different irradiation time. B) A plot of the mean fluorescence intensity extracted from the CLSM images as a function of irradiation time. Scale bar: 20 μm.

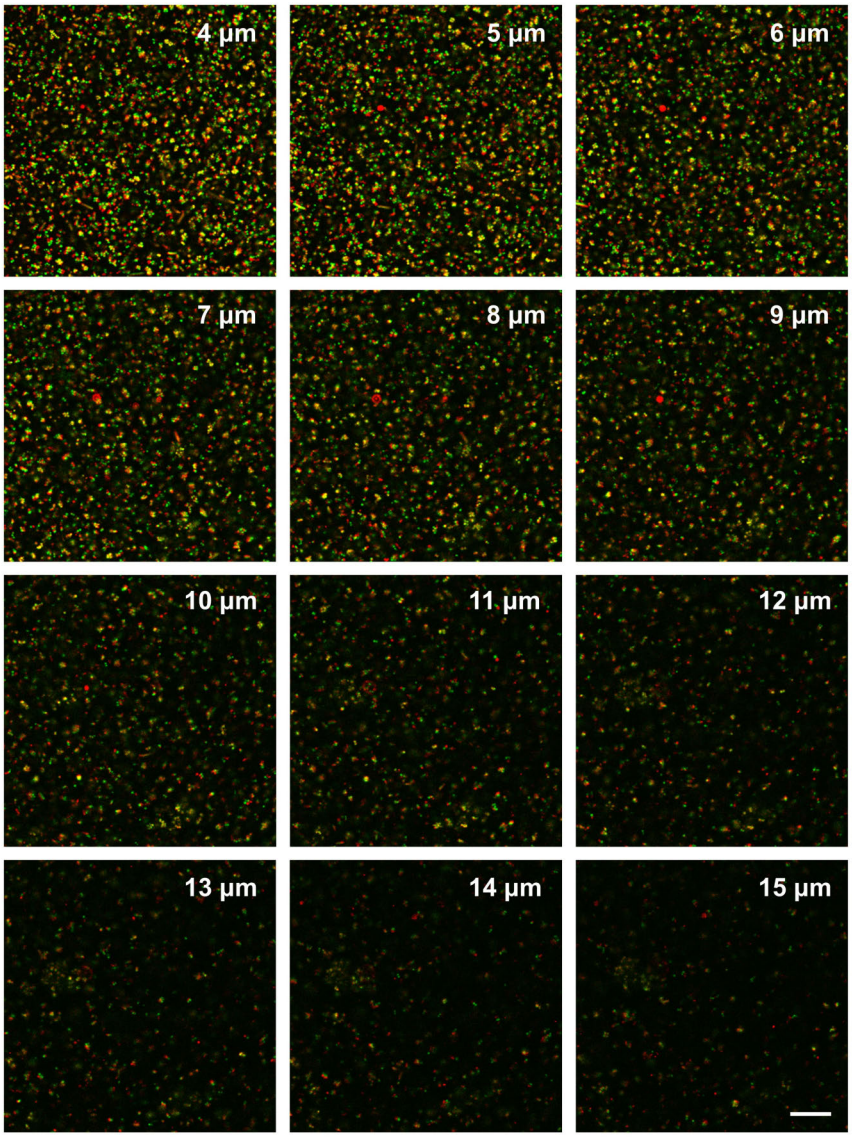

Figure S22. Spatial distribution of Poly−TICT@AIE and the bacteria within a MRSA biofilm. Poly−TICT@AIE is shown in red, and the bacteria was stained with SYTO 9 and is shown in green. Scale bar: 20 μm.

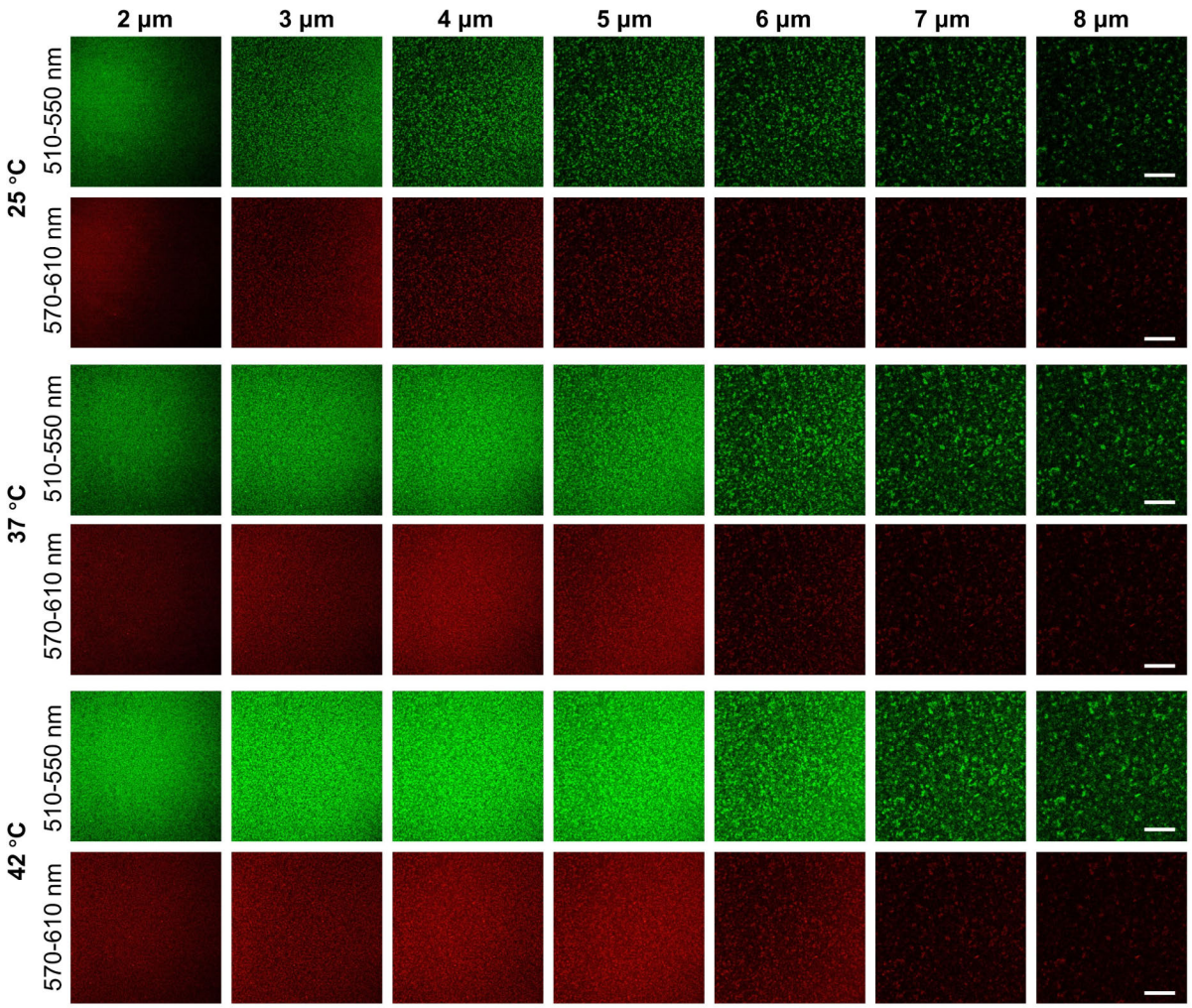

Figure S23. CLSM images of Poly−TICT@AIE within a MRSA biofilm at different temperatures. Scale bar: 50 μm.

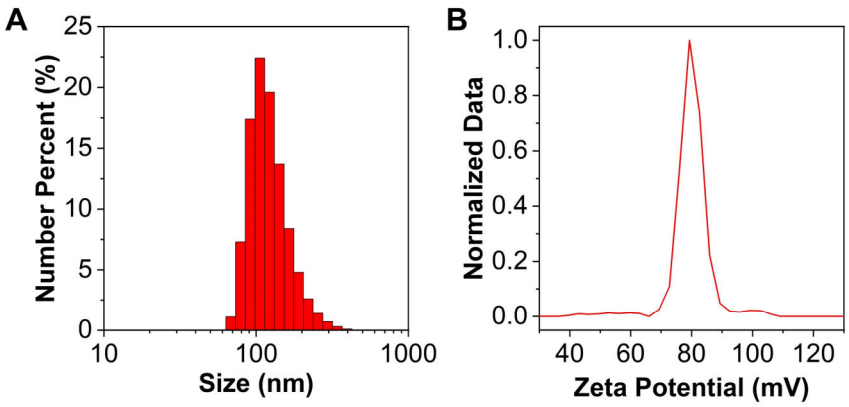

Figure S24. Particle size distribution and zeta potential of Poly–TICT@AIE(+). A) Particle size distribution. B) A plot of zeta potential.

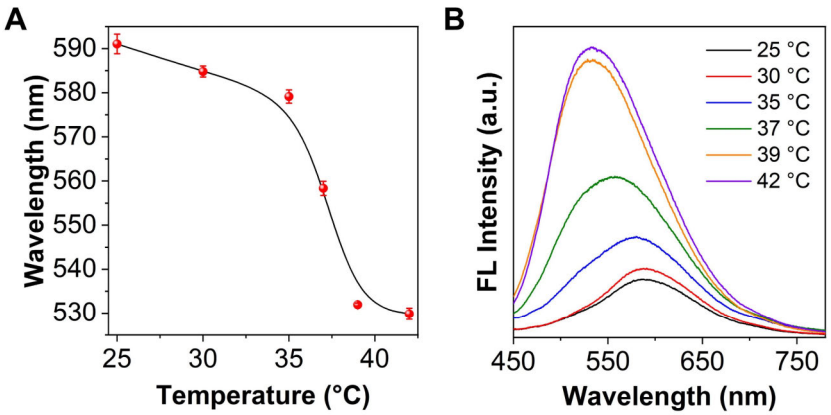

Figure S25. The spectral responses of Poly–TICT@AIE(+) to temperature variation. A) A plot of the emission maximum of Poly–TICT@AIE(+) as a function of temperature. B) Emission spectra of Poly–TICT@AIE(+) at different temperatures. Ex = 405 nm.

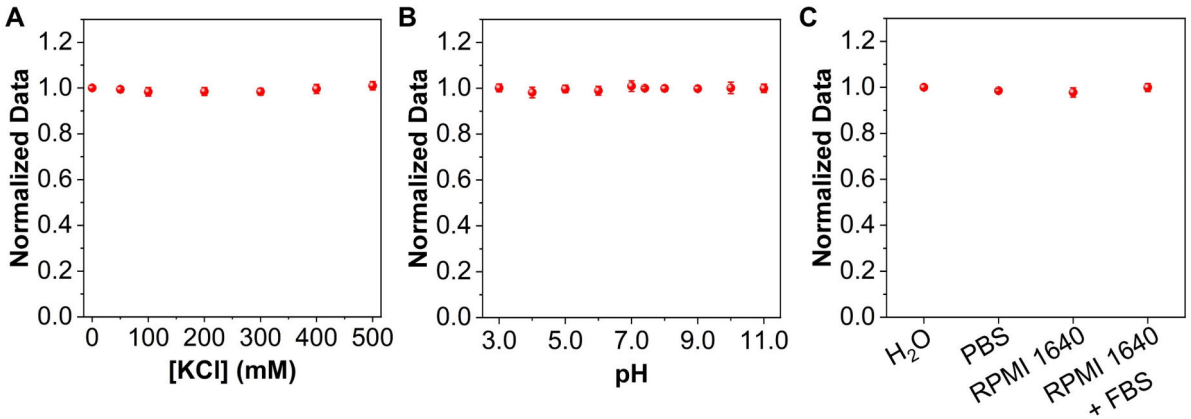

Figure S26. The impacts of different parameters on the fluorescence properties of Poly–TICT@AIE(+) at 25 °C. A) The normalized fluorescence intensity of Poly–TICT@AIE(+) at 590 nm in the presence of different concentrations of KCl. (B) The normalized fluorescence intensity of Poly–TICT@AIE(+) at 590 nm under different pH values. C) The normalized fluorescence intensity of Poly–TICT@AIE(+) at 590 nm in different media. Ex = 470 nm.

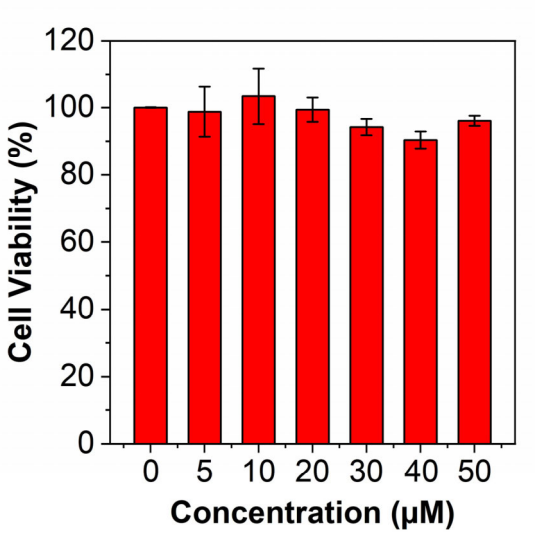

Figure S27. Cell viability of A549 cells incubated with different concentrations of Poly−TICT@AIE(+).

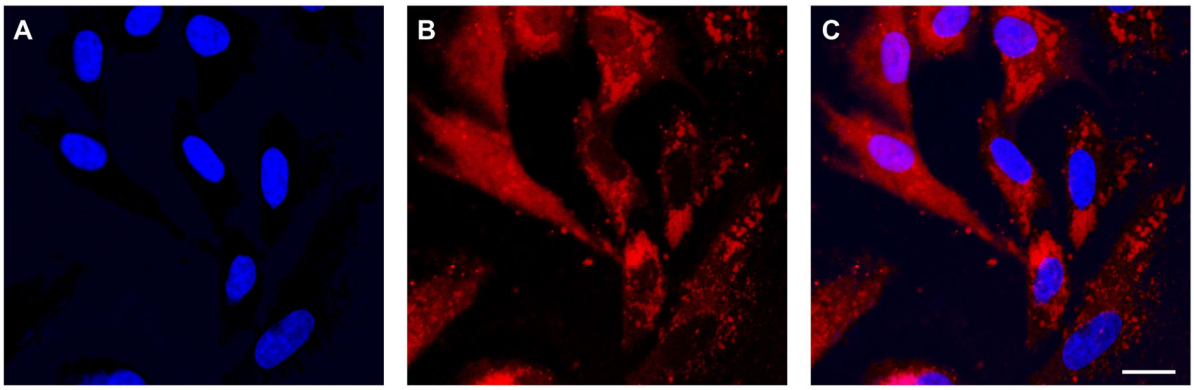

Figure S28. CLSM images of A549 cells incubated with Poly–TICT@AIE(+). A) Fluorescence channel for Hoechst 33342 (shown in blue). Ex = 405 nm, Em = 420–480 nm. B) Fluorescence channel for Poly–TICT@AIE(+) (shown in red). Ex = 488 nm, Em = 540–620 nm. C) The overlaid image. Scale bar: 20 μm.

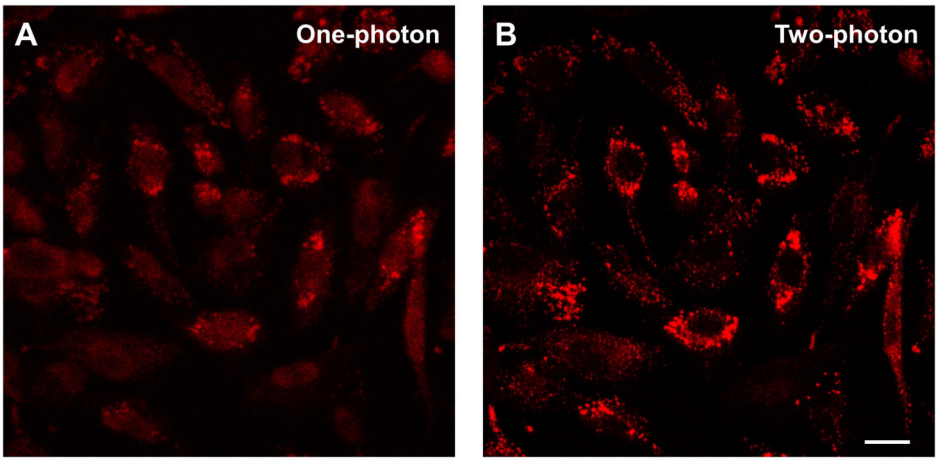

Figure S29. CLSM images of A549 cells incubated with Poly–TICT@AIE(+). A) One-photon image. Ex = 405 nm; Em = 540–620 nm. B) Two-photon image. Ex = 840 nm; Em = 540–620 nm. Scale bar: 50 μm.

Table S1. Emission maximum, integral area, and fluorescence lifetime (τ) of Poly−TICT@AIE at different temperatures.

Temperature (°C)	Wavelength (nm)	Integral area (× 10^4)	τ (ns)
25	591.4 ± 1.2	8.17 ± 0.03	2.06 ± 0.06
30	585.5 ± 1.0	9.74 ± 0.02	1.96 ± 0.04
35	574.6 ± 0.9	13.29 ± 0.06	1.72 ± 0.07
37	556.1 ± 1.9	20.17 ± 0.14	1.27 ± 0.11
39	533.1 ± 1.1	27.87 ± 0.30	1.04 ± 0.07
42	527.6 ± 1.1	30.18 ± 0.05	0.95 ± 0.04

Table S2. Thermometric performance of Poly−TICT@AIE at different temperatures.

Temperature (°C)	Spectral position		Integral area		Fluorescence lifetime	
	S_r^{λ} (% °C^{-1})	δT (°C)	S_r^{I} (% °C^{-1})	δT (°C)	S_r^{τ} (% °C^{-1})	δT (°C)
30	0.20	0.86	3.23	0.07	1.02	2.00
35	0.38	0.40	5.34	0.08	2.79	1.46
37	1.67	0.20	17.06	0.04	17.72	0.49
39	2.15	0.10	13.80	0.08	11.06	0.61
42	0.35	0.60	2.55	0.06	3.16	1.33

Table S3. Fluorescence lifetime and pre-exponential factors of Poly−TICT@AIE at different temperatures.

Temperature (°C)	A_1	τ_1 **(ns)**	A_2	τ_2 **(ns)**	τ **(ns)**	χ^2
25	0.12 ± 0.025	4.03 ± 0.41	0.88 ± 0.020	0.84 ± 0.06	2.06 ± 0.06	0.997
30	0.11 ± 0.007	3.85 ± 0.17	0.89 ± 0.042	0.78 ± 0.03	1.96 ± 0.04	0.999
35	0.10 ± 0.028	3.60 ± 0.36	0.90 ± 0.015	0.77 ± 0.04	1.72 ± 0.07	0.998
37	0.04 ± 0.006	4.04 ± 0.52	0.96 ± 0.048	0.64 ± 0.04	1.27 ± 0.11	0.997
39	0.02 ± 0.000	3.89 ± 0.16	0.98 ± 0.058	0.52 ± 0.01	1.04 ± 0.07	0.998
42	0.02 ± 0.001	3.83 ± 0.23	0.98 ± 0.093	0.51 ± 0.01	0.95 ± 0.04	0.998

Table S4. Fluorescence lifetime of Poly–TICT@AIE in the MRSA biofilm at different temperatures.

Temperature (°C)	τ **(ns)**
25	2.43 ± 0.09
37	1.57 ± 0.01
42	1.49 ± 0.02

Table S5. Comparison of different fluorescent nanothermometers for temperature sensing.

Nanothermometer	Parameter	S_r^{max} (% °C^{-1})	T_m (°C)	δT (°C)	ΔT (°C)	Ref
Composite structures						
Poly−TICT@AIE	SP	2.15	39	0.10	25–42	This
	FI	17.06	37	0.04		work
	FL	17.72	37	0.49		
TRF NPs	FI ratio	2.37	65	–	25–65	3
Inorganic materials						
Ag_2S-PEG	SP	0.12	25	–	25–75	4
	FI	5.00	25	–	25–80	
	FI ratio	1.40	25	–	25–80	
$Y_3(Al,Ga)_5O_{12}$:0.1%Pr	FI ratio	3.60	–36	0.02	–256–427	5
phosphors	FL	1.50	207	–	37–277	
$LiLaP_4O_{12}$:1%Nd nanocrystals	SP	0.47	50	1.05	–190–327	6
TTA-UCNPs + $NaYF_4$:Nd	FI ratio	7.10	22	0.10	10–50	7
QD655	FI ratio	6.30	41	0.10	31–41	8
Au nanoclusters	FI	–	–	0.10–0.30	10–45	9
	FL	–	–	0.30–0.50	14–43	
Fluorescent proteins						
emGFP-Mito	SP	2.20	23	0.26	23–39	10
gTEMP	FI Ratio	1.15	34	0.10	5–50	11
Organic dyes						
ER thermo yellow	FI	3.90	37	0.40	32–37	12
Mito thermo yellow	FI	2.00–2.80	42	–	37–42	13
Mito-RTP	FI ratio	2.72	41	0.60	34–41	14
Thermoresponsive synthetic polymers						
Anionic nanogel FPT	FI	–	–	0.29–0.50	27–33	15
Cationic nanogel FPT	FI	–	–	0.02–0.40	20–40	16
	FL	–	–	0.11–0.84		
Anionic linear FPT	FL	–	–	0.18–0.58	29–39	17
Cationic linear FPT	FL	–	–	0.30–1.29	25–35	18
	FI ratio	–	–	0.01–0.25	25–44	19

Note: S_r^{max}, maximum relative thermal sensitivity; T_m, the temperature at which S_r^{max} was obtained; δT, the temperature resolution or temperature uncertainty; ΔT, temperature sensing range; SP, spectral position; FI, fluorescence intensity; FL, fluorescence lifetime; FI ratio, fluorescence intensity ratio; FPT, fluorescent polymeric thermometer.